Photodissociation Dynamics of Allyl Alcohol at 193 nm

Tae Yeon Kang, Seung Keun Shin, and Hong Lae Kim*

Department of Chemistry and Basic Science Research Institute, Kangwon National University, Chuncheon 200-701, Korea

Received: May 8, 2003; In Final Form: September 15, 2003

Photodissociation of allyl alcohol at 193 nm has been investigated by measuring laser-induced fluorescence spectra of OH fragments that are exclusively produced in the ground ($^2\Pi$) electronic state. From the spectra, rotational and vibrational population distributions in OH and energy partitioning among fragments have been obtained. The measured average rotational energies in OH are 1430/1320 cm^{-1} and the vibrational population ratio is 0.89/0.11 for $v = 0/1$, respectively. In addition, no polarization dependences upon dissociation have been observed. It is suggested that the dissociation takes place in the excited triplet surface via curve crossing from the initial $\pi \rightarrow \pi^*_{C=C}$ transition.

Introduction

Studies of photodissociation dynamics are of fundamental importance in understanding electronic structures and potential energy surfaces of molecules in the excited state because the dissociation dynamics is governed by the nature and shape of the surfaces. For example, an electronic transition such as in UV to an excited electronic state can induce impulsive dissociation from a pure repulsive surface or predissociation from a surface where couplings between the surfaces exist.[1] On the other hand, emission spectra of dissociating molecules reflect the Franck−Condon overlap of vibrational wave functions between the excited and the ground electronic states, from which the molecular structures in the dissociative excited state can be deduced.[2,3] Thus, by studying the absorption and emission spectra and/or studying the photodissociation dynamics, one can explore the shape of the excited-state potential energy surfaces correlating to the individual reaction products.

Photodissociation dynamics of compounds containing C═C double bonds is of considerable interest because these molecules, upon UV irradiation, can produce not only molecular products via molecular elimination pathways but also radical products via simple bond cleavages. The photodissociation dynamics of haloethylenes has particularly been investigated both experimentally and theoretically. The UV absorption around 190−200 nm is assigned as the $\pi \rightarrow \pi^*$ transition, from which the dissociation takes place. Photodissociation dynamics of chloroethylene excited at 193 nm was thoroughly investigated using photofragment translational spectroscopy and Doppler broadened resonance-enhanced multiphoton ionization spectroscopy of H, Cl, H_2, and HCl fragments, where energy distributions and polarization dependences upon dissociation were measured.[4−8] It was concluded from the experimental results that the dissociation takes place in the ground electronic state after internal conversion from the initially excited state including a small amount of direct elimination of Cl from the excited state. In addition, it was found from the measured product branching ratio, Cl/HCl, that molecular elimination of HCl is the major dissociation channel. The dissociation mechanisms of chloroethylene were quantum chemically investigated by Morokuma and co-workers.[9] Ab initio molecular orbital calculations on the energies and structures of the transition states for individual reaction pathways showed that the major reaction pathway would be the 1,1 molecular elimination of HCl producing vinylidene which subsequently isomerizes into acetylene. Cyanoethylene (acrylonitrile) is another prototypical molecule for substituted ethylenes, whose photochemistry has been investigated. Blank et al. examined the photodissociation dynamics of acrylonitrile at 193 nm by photofragment translational spectroscopy.[10] From the measured translational energy distributions of H, H_2, CN, and HCN fragments, they concluded that rapid internal conversion to the ground electronic state occurs followed by elimination of those four fragments. From the product branching ratio and the calculated RRKM dissociation rates, 2×10^{-4} (CN/HCN channel), the molecular elimination channels were identified to be the major channels. In addition, the measured translational energy distributions reflect statistical simple bond rupture for the radical channels while the molecular elimination channels have substantial recombination barriers. These dissociation channels have been identified by ab initio molecular orbital calculations and the branching ratios estimated by RRKM rates are in good agreement with the measurements.[11] Upon absorption at 193 nm, the CN radical elimination channel from acrylonitrile was also investigated using transient frequency-modulation spectroscopy.[12] The measured quantum yield was 0.003, implying that this channel is minor and the translational energy distribution measured from the Doppler profiles was well fit by the statistical prior calculation, from which it was concluded that the dissociation takes place in the ground electronic state after internal conversion.

Photodissociation dynamics of C_3H_5X (X = Cl, I, CN) upon UV irradiation, particularly at 193 nm, has recently been reported. In these molecules that have one more skeletal carbon atom than ethylene resulting in various conformational isomers, many more dissociation channels can be opened than those in substituted ethylenes. The electronic transitions around 200 nm are the similar $\pi \rightarrow \pi^*$ transition to chloroethylene, but considerable amount of $n\sigma^*$ character is incorporated especially in the gauche conformers of allyl chloride.[13,14] As a result, the dissociation dominantly takes place in the excited electronic state along nonadiabatic potential surfaces and the branching ratio

* Corresponding author. E-mail: hlkim@cc.kangwon.ac.kr.

10.1021/jp030589z CCC: $25.00
Published on Web 11/15/2003

Cl/HCl is increased in the photodissociation of allyl chloride compared to chloroethylene. For compounds containing CN, the radical production channels were particularly investigated. It has been found from allyl cyanide excited at 193 nm that CN radicals are mainly produced from the ground electronic state via internal conversion from the initial $\pi \rightarrow \pi^*$ transition and that the dissociation dynamics was successfully modeled by statistical theories.[15] A study of the photodissociation of 2-butenenitrile at 193 nm demonstrated another example of statistical ground-state unimolecular dissociation.[16] In the latter study, frequency-modulated diode laser absorption spectroscopy was employed to measure the translational energy distribution from Doppler profiles in the spectra of CN fragments. In particular, ab initio calculations estimate H atom migration before the CN elimination from 2-butenenitrile resulting in CN and an allyl radical products rather than a propenyl radical product. Very recently, however, emission spectra of allyl alcohol from the dissociative excited state at 199 nm were reported, from which predissociation or an electronic curve crossing was proposed for the dissociation mechanism.[17] The $\pi \rightarrow \pi^*$ transition is responsible for the transition at this wavelength, but a little of Rydberg character is estimated from the ab initio calculations. The dissociation dynamics would be different for substituents resulting from different characters of the excited state and the shape of the potential energy surfaces leading to particular fragments.

In this article, photodissociation dynamics of allyl alcohol at 193 nm has been investigated by measuring rotationally resolved laser-induced fluorescence spectra of OH fragments. Product energy partitioning, Λ-doublet distribution and spin−orbit population ratio of the OH fragments as well as polarization dependences upon dissociation have been measured, from which the detailed dissociation dynamics of the OH radical product channel is discussed.

Experiments

The experiments were performed in a flow cell with conventional pump−probe geometry. The cell was evacuated to a pressure of about 10^{-3} Torr and the gaseous sample was continuously flowed through the cell at a pressure of 10 mTorr whose pressure was controlled by needle valves. The liquid sample stated purity of 99% was purchased from Aldrich and used without further purification.

The photolysis light at 193 nm polarized with a stack of quartz plates was obtained from an ArF excimer laser (Lambda Physik Lextra 50). The excimer laser beam was shaped as a circle (~5 mm diameter) with an aperture, and the power was kept as low as possible (5 mJ/pulse) to avoid any multiphoton effect. The horizontally polarized probe light to measure the laser-induced fluorescence (LIF) spectra of OH fragments was a frequency-doubled output of a dye laser (Lumonics HD-500, 20 μJ/pulse) pumped by the second harmonic of an Nd:YAG laser. The laser beams were introduced to the cell through arms in which baffles were placed to minimize the scattered radiation into a detector. The two laser beams were collinearly counterpropagated through the cell or introduced at a right angle to obtain two different experimental geometries with a pump−probe delay time of about 100 ns. The 10 mTorr sample pressure and 100 ns delay time ensure that the nascent product quantum state distributions were probed. The LIF spectra of OH were measured employing the (0,0) and (1,1), A ← X vibronic transition in the region around 306−325 nm. The induced fluorescence was measured with a photomultiplier tube (Hamamatsu, R212U) at a right angle to the two laser beams through appropriate cutoff filters.

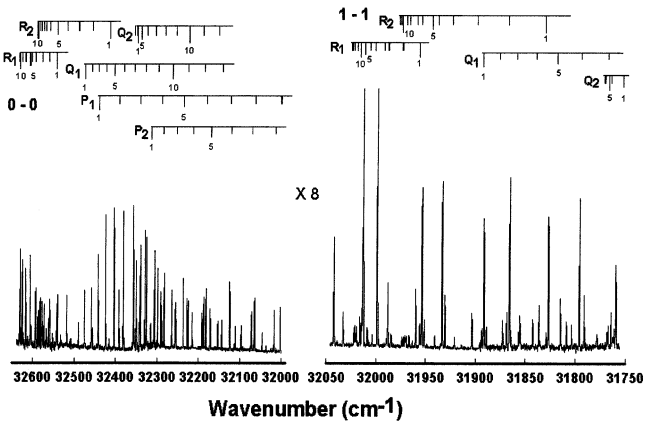

Figure 1. Laser-induced fluorescence spectra of OH produced from photodissociation of allyl alcohol at 193 nm employing the A ← X electronic transition.

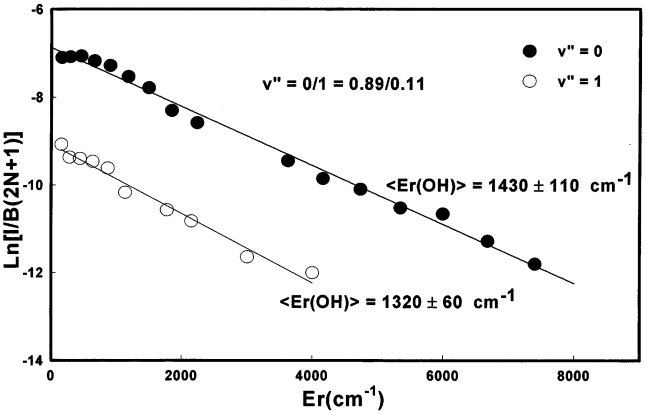

Figure 2. Boltzmann plots of the rotational distributions obtained from the spectra in Figure 1.

The detected signals were fed to boxcars and processed in a signal processor and PC. The powers of the photolysis and the probe lights were separately measured using photodiodes and the measured fluorescence spectra were corrected with variation of laser intensities.

To measure translational energies of OH from the Doppler broadening in the spectra, the laser line width was first measured. The LIF spectrum of $P_1(4)$ rotational branch transition in OH was measured after translational relaxation by collisions with 5 Torr of Ar at 2 μs pump−probe delay. The measured line profiles were essentially the same at longer than 2 μs or higher Ar pressures. Thus, we assume the laser line profile should be the same as the measured line profile under this condition, which fitted well to Lorentzian with 0.17 cm^{-1} at fwhm. This line profile is used for translational energy measurements after deconvolution from the Doppler profiles.

Results and Discussion

Measured LIF spectra of OH from photodissociation of allyl alcohol at 193 nm are presented in Figure 1. Rotational transitions in the 0−0, and 1−1 vibrational bands are clearly observed and assignments are given on top of the spectra according to rotational angular momentum couplings governed by Hund's case (b).[18] Rotational population distributions are obtained from relative intensities of the peaks corrected by appropriate line strength factors.[19] From the Boltzmann-type plots, rotational temperatures are measured to be 2050 and 1900 K (Figure 2) and thus measured average rotational energies in OH are 1430 ±110 and 1320 ± 60 cm^{-1} for $v'' = 0$ and 1,

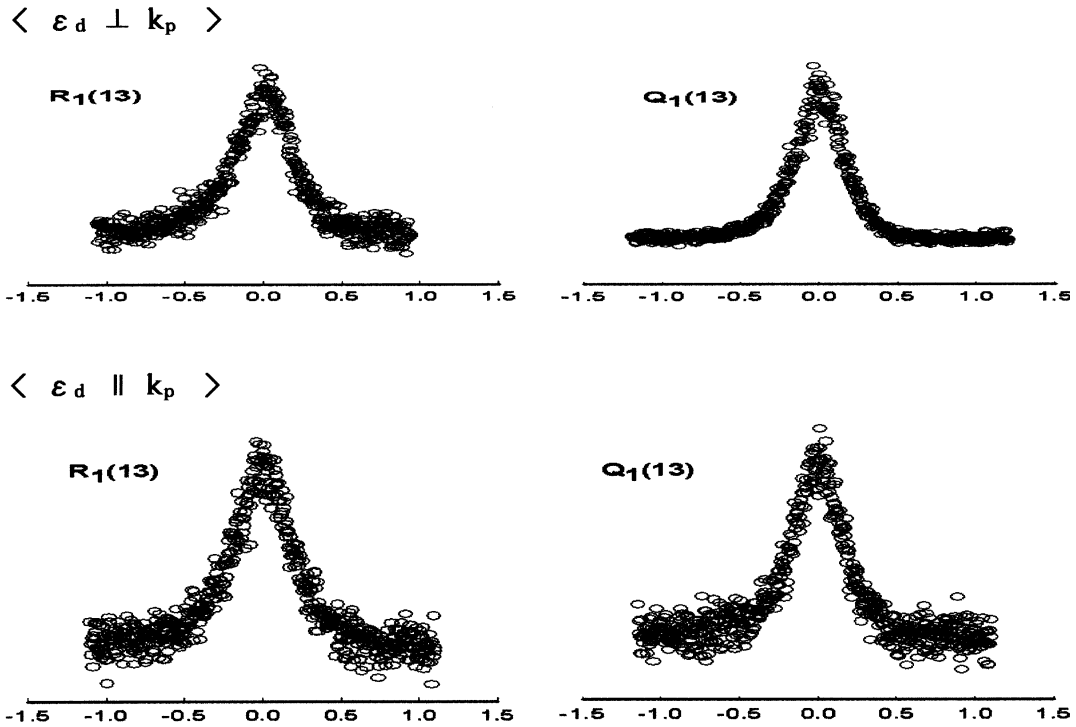

Figure 3. Doppler profiles of the rotationally resolved spectra of OH at the rotational quantum number $N = 13$ under two different experimental geometries described in the Experimental Section.

respectively. In addition, the vibrational population distribution is obtained from integrated intensities of the peaks from the 0−0 and 1−1 rovibrational transitions employing reported Franck−Condon factors,[20] which is 0.89/0.11 for $v'' = 0/1$.

In Figure 3, the Doppler broadened spectra for the $R_1(13)$ and $Q_1(13)$ rotational branch transitions under different experimental geometries mentioned in the Experimental Section are presented. Maximum absorption of dissociating light by the molecule takes place when the transition dipole moment of the molecule lies along the electric vector of the linearly polarized dissociating light. Thus, Doppler profiles of absorption spectra of the recoiling fragments measured relative to the direction of the polarization vector of the dissociating light in the laboratory frame reveal the angular distribution of the fragments, assuming the dissociation takes place faster than a rotational period of the parent molecule. In general, when the dissociation is slow, the angular distribution would be isotropic, which results in Gaussian-like Doppler profiles, whereas for fast dissociation, the anisotropic angular distribution results in a unique shape of the Doppler profiles.[21,22] The measured profiles are essentially the same, Gaussian-like implying no polarization dependences upon dissociation. Thus, average translational energies of the OH fragment have been measured from the second moment of the profiles assuming isotropic, Gaussian velocity distributions. A typical Doppler broadened spectrum of OH is presented in Figure 4 for the $P_1(2)$ rotational branch transition. The second moment of the profile was measured after deconvolution of the laser line profile, from which the translational energy of 5800 ± 300 cm^{-1} was obtained. The calculated center of mass translational energy releases are then 7900 ± 900 cm^{-1} for $N = 2$. The translational energy releases for several N values were measured and listed in Table 1. It is noticeable in the table that relatively invariant translational energy releases were observed for OH at different rotational states.

In Figures 5 and 6, the spin−orbit population ratio (F1/F2, $^2\Pi_{3/2}/^2\Pi_{1/2}$) and the Λ-doublet distribution also measured from the spectra as a function of rotational quantum numbers are

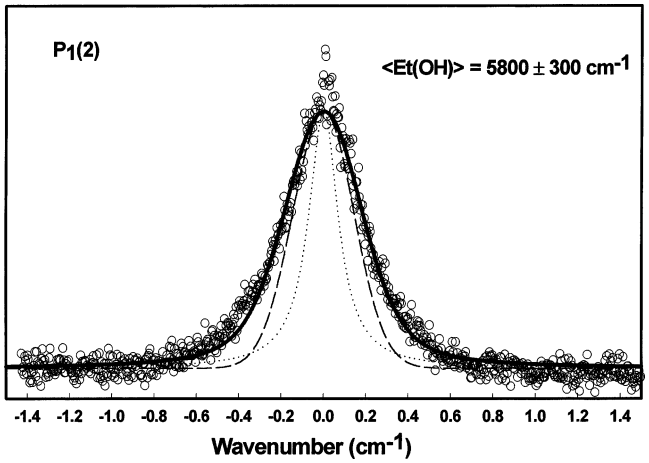

Figure 4. A typical Doppler profile of OH for the $P_1(2)$ rotational branch transition. The dotted line represents the laser line profile. The dashed line is the measured line profile after deconvolution of the laser line profile.

presented. The spin−orbit population ratio has the average value of 1.3 ± 0.3, showing a slight propensity for the higher spin−orbit state, whereas the Λ-doublet distribution shows a statistical distribution. One might argue that in a classical sense, when the dissociation time is fast, faster than the electron precession, then a statistical population distribution between the angular momentum states would be expected. However, when the dissociation is slow, a nonstatistical population distribution is expected according to the correlation. The preference of OH being in the higher angular momentum state could be explained if the detailed shape of potential surface in the excited state would be known.

To figure out the dissociation dynamics, absorption and emission spectra and their spectral assignments are extremely helpful. The spectrum evidences a continuous absorption starting from 220 nm and peaks around 200 nm. The emission spectra of the dissociating molecules upon excitation at 199.7 nm show

TABLE 1: Product Energy Partitioning (in cm^{-1}) from Photodissociation of Allyl Alcohol at 193 nm

	measured	prior I	prior II
E_{av}[a]	24980		
$<E_t(OH)>$	1430 ± 110	1950	1620[b]
$E_t(N)$			
$N = 1$	8800 ± 1400	3510	8700[c]
$N = 2$	7900 ± 900	3500	8690[c]
$N = 3$	8300 ± 1400	3490	8680[c]
$N = 5$	8500 ± 1300	3450	8640[c]
$N = 13$	7800 ± 1300	3140	8320[c]

[a] $E_{av} = h\nu(51810\ cm^{-1}) - D_0\ (27960\ cm^{-1}) + E_{int}(C_3H_5OH$ at 300 K, 1130 $cm^{-1}) = 24980\ cm^{-1}$. [b] Calculated at $E_{av} = 19180\ cm^{-1}$ which is obtained by subtraction of the estimated exit channel barrier(5800 cm^{-1}) from the total available energy. [c] Obtained from the prior calculation plus the exit channel barrier assuming the barrier energy is transformed into product translation.

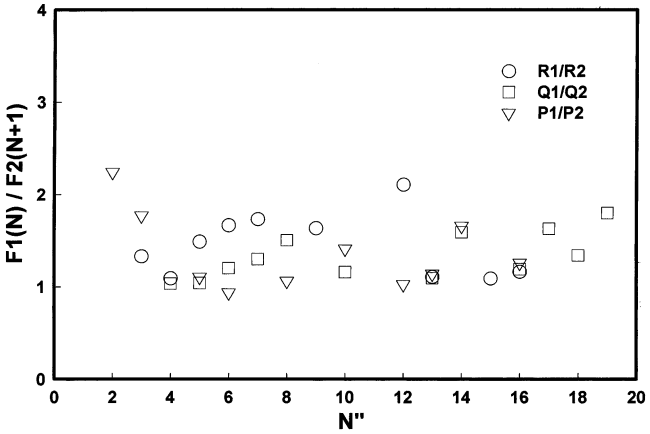

Figure 5. F1/F2 spin−orbit population distribution of OH obtained from the spectra in Figure 1.

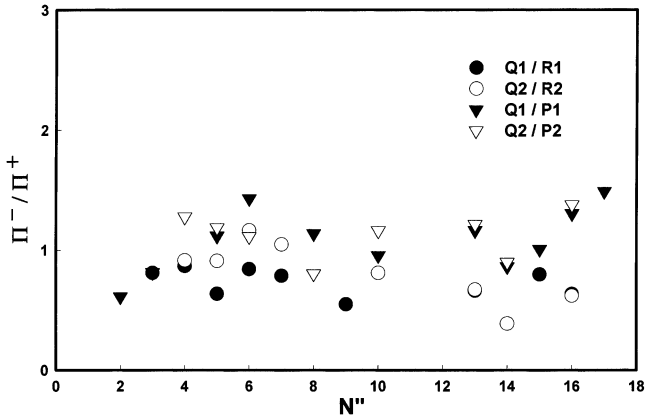

Figure 6. Λ-doublet distribution of OH obtained from the spectra in Figure 1.

vibrational transitions associated with the C=C stretching and the CH_2 torsion with considerable intensities, which implies a geometrical change in the Franck−Condon region of the potential energy surfaces upon initial excitation. With an aid of ab initio calculations and the emission spectra, it has been concluded that the transition responsible for the peak should be $\pi \rightarrow \pi^*_{C=C}$ with negligible contributions from the n_O and σ^* character and hence the dissociation into allyl and OH radicals should proceed via an electronic curve crossing or predissociation.[17]

Another helpful piece of information for understanding the dissociation dynamics is spin correlation. According to the correlation arguments, the present two doublet ground-state products are correlated to the four parent molecular states that are three excited triplet and one ground singlet states. Since the excited singlet state resulting from the present $\pi \rightarrow \pi^*$ transition correlates to either one of the product radicals being in the excited state, the dissociation should take place from either the ground singlet state or the excited triplet states. Thus, it can be concluded that the electronic transition at 193 nm leads this molecule to the excited singlet state followed by either internal conversion to the ground state or electronic curve crossing to the triplet state, from which the dissociation takes place. In the case of acrylonitrile[12] and allyl cyanide,[15] the dissociation in the ground state after internal conversion was suggested.

The dissociation dynamics can also be understood by examining the energy partitioning, which can be predicted by applying some dissociation models. From the zero-point energies and the heat of formations of the allyl radical, OH, and allyl alcohol, the dissociation energy is calculated to be 27 960 cm^{-1}. Then, the available energy that can be distributed among products is 24 980 cm^{-1} calculated from the photon energy at 193 nm and internal energy of the parent molecule at ambient temperature. Although it is an extreme case of the dissociation model, a statistical model was applied to obtain the energy distributions when the dissociation occurs in the vibrationally hot ground state after internal conversion. Thus, a prior model was employed to obtain the translational and rotational energy distributions of OH.[23,24] In this model, it is assumed that the available energy should be distributed among all degrees of freedom of the products with equal probability. Thus, the rotational population at the individual rotational state of OH would be proportional to the number of accessible quantum states of the allyl radical at the energy, $E = E_{avail} - E_{OH}$ (v, J). The vibrational frequencies and the rotational constants of the allyl radical were obtained by ab initio calculations using the Gaussian 98 program package (6-31G**(d,p), MP2 level)[25] and the number of quantum states was directly counted. The translational energy distributions were also calculated from the same prior model. For a fixed OH(v, J), the translational prior was calculated by counting the number of quantum states in the allyl radical at the energy $E = E_{avail} - E_t - E_{OH}$ (v, J) and the average translational energy was calculated from the prior distribution. The average rotational energy from the calculated distribution does not agree well with the experiment. Moreover, the calculated average translational energies from the model substantially deviate from the experimental results (Table 1). These imply that the dissociation should at least occur faster than energy randomization, where it is in general assumed for the dissociation from the vibrationally hot ground state after the internal conversion. One might think of a dynamical effect such as a barrier in the exit channel in the course of dissociation, whose energy can mainly be transformed into product translation. In the present case, however, it is very unlikely that there may be a considerable reverse barrier for recombination of the two radicals.

The photodissociation of allyl alcohol should take place in the excited triplet state via electronic curve crossing. A well may exist on the surface where the molecule reaches upon initial excitation and the triplet state that crosses at some point is strongly dissociative. There may be a conical intersection on the potential energy surface along the reaction coordinate and a barrier from crossing or from weak interaction between the singlet and triplet states in the exit channel. In this case, a large portion of the product translational energies comes from the exit channel barrier, and the remaining available energy would be statistically distributed among product degrees of freedom,

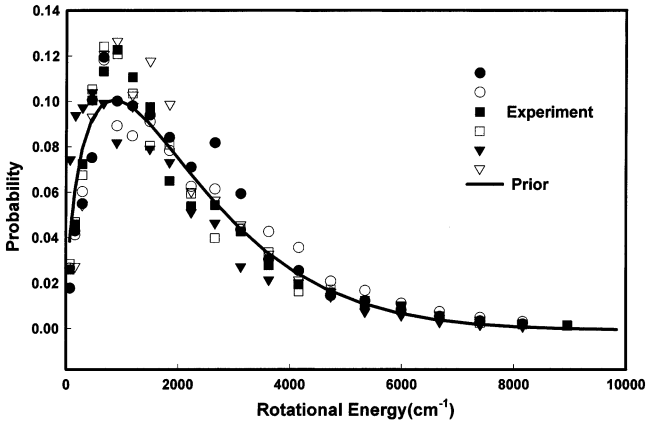

Figure 7. Rotational population distributions of OH in the $v'' = 0$ level measured from the experiment and from the statistical prior calculations.

assuming that the initially excited molecule spends enough time in the well before the crossing, probably several rotational−vibrational periods for the energy to be randomized. Similar mechanisms have been suggested for the photodissociation of acetaldehyde[26] and acetyl cyanide[27] excited by irradiation of the UV light. The directional memory, such as the transition dipole moment, can then be lost upon rotation of the parent molecule, which results in no polarization dependences and a statistical distribution of Λ-doublets observed in the present experiment. Assuming the reverse barrier of some 5800 cm^{-1}, the average translational energy releases and rotational energy distributions were recalculated using the same prior model, which agree rather well with the experiments (Figure 7 and Table 1).

In conclusion, the photodissociation of allyl alcohol at 193 nm takes place in the excited triplet state via electronic curve crossing from the initial $\pi \rightarrow \pi^*$ transition, although it would be extremely helpful to clarify definitely the mechanism of the reaction in detail if the potential energy surfaces in the excited state were theoretically known.

Acknowledgment. This work was financially supported by the Korea Science and Engineering Foundation.

References and Notes

(1) Schinke, R. *Photodissociation Dynamics*; Cambridge University Press: Cambridge, 1993.

(2) Imre, D.; Kinsey, J. L.; Sinha, A.; Krenos, J. *J. Phys. Chem*. **1984**, *88*, 3956.

(3) Browning, P. W.; Jensen, E.; Waschewsky, G. C. G.; Tate, M. R.; Butler, L. J.; Hessler, J. P. *J. Chem. Phys*. **1994**, *101*, 5652.

(4) Reilly, P. T. A.; Xie, Y.; Gordon, R. J. *Chem. Phys. Lett*. **1991**, *178*, 511.

(5) Mo, Y.; Tonokura, K.; Matsumi, Y.; Kawasaki, M.; Sato, T.; Arikawa, T.; Reilly, P. T. A.; Xie, Y.; Yang, Y.; Huang, Y.; Gordon, R. J. *J. Chem. Phys*. **1992**, *97*, 4815.

(6) Huang, Y.; Yang, Y.; He, G.; Gordon, R. J. *J. Chem. Phys*. **1993**, *99*, 2752.

(7) Huang, Y.; He, G.; Yang, Y.; Hashimoto, S.; Gordon, R. J. *Chem. Phys. Lett*. **1994**, *229*, 621.

(8) Blank, D. A.; North, S. W.; Stranges, D.; Suits, A. G.; Lee, Y. T. *J. Chem. Phys*. **1997**, *106*, 539.

(9) Riehl, J.-F.; Morokuma, K. *J. Chem. Phys*. **1994**, *100*, 8976.

(10) Blank, D. A.; Suits, A. G.; Lee, Y. T.; North, S. W.; Hall, G. E. *J. Chem. Phys*. **1998**, *108*, 5784.

(11) Derecskei-Kovacs, A.; North, S. W. *J. Chem. Phys*. **1999**, *110*, 2862.

(12) North, S. W.; Hall, G. E. *Chem. Phys. Lett*. **1996**, *263*, 148.

(13) Browning, P. W.; Kitchen, D. C.; Arendt, M. F.; Butler, L. J. *J. Phys. Chem*. **1996**, *100*, 7765.

(14) Myers, T. L.; Kitchen, D. C.; Hu, B.; Butler, L. J. *J. Chem. Phys*. **1996**, *104*, 5446.

(15) Oh, C. Y.; Shin, S. K.; Kim, H. L.; Park, C. R. *Chem. Phys. Lett*. **2001**, *342*, 27.

(16) Li, R.; Derecskei-Kovacs, A.; North, S. W. *Chem. Phys*. **2000**, *254*, 309.

(17) Parsons, B. F.; Szpunar, D. E.; Butler, L. J. J. *Phys. Chem. A* **2000**, *104*, 10669.

(18) Dieke, G. H.; Crosswhite, H. M. *J. Quant. Spectrosc. Radiat. Transfer* **1962**, *2*, 97.

(19) Chidsey, I. L.; Crosley, D. R. *J. Quant. Spectrosc. Radiat. Transfer* **1980**, *23*, 187.

(20) Luque, J.; Crosley, D. R. *J. Chem. Phys*. **1998**, *109*, 439.

(21) Zare, R. N.; Herschbach, D. R. *Proc. IEEE* **1963**, *51*, 173.

(22) Hall, G. E.; Houston, P. *Annu. Rev. Phys. Chem*. **1989**, *375*, 40

(23) Zamir, E.; Levin, R. D. *Chem. Phys*. **1980**, *52*, 253.

(24) Levine, R. D.; Bernstein, R. B. *Molecular Reaction Dynamics and Chemical Reactivity*; Oxford University Press: New York, 1987.

(25) Frisch, M. J.; Trucks, G. W.; Schlegel, H. B.; Scuseria, G. E.; Robb, M. A.; Cheeseman, J. R.; Zakrzewski, V. G.; Montgomery, J. A.; Stratmann, R. E.; Burant, J. C.; Dapprich, S.; Millam, J. M.; Daniels, A. D.; Kudin, K. N.; Strain, M. C.; Farkas, O.; Tomasi, J.; Barone, V.; Cossi, M.; Cammi, R.; Mennucci, B.; Pomelli, C.; Adamo, C.; Clifford, S.; Ochterski, J.; Perdersen, G. A.; Ayala, P. Y.; Cui, Q.; Morokuma, K.; Malick, D. K.; Rabuck, A. D.; Raghavachari, K.; Foresman, J. B.; Cioslowski, J.; Ortiz, J. V.; Stefanov, B. B.; Liu, G.; Liashenko, A.; Piskorz, P.; Komaromi, I.; Gomperts, R.; Martin, R. L.; Fox, D. J.; Keith, T.; Al-Laham, M. A.; Peng, C. Y.; Nagayakkara, A.; Gonzales, C.; Challacombe, M.; Gill, P. M. W.; Johnson, B. G.; Chen, W.; Wong, M. W.; Andres, J. L.; Head-Gordon, M.; Replogle, E. S.; Pople, J. A. *Gaussian* 98; Gaussian Inc.: Pittsburgh, PA, 1998.

(26) Gejo, T.; Takayanagi, M.; Kono, T.; Hanazaki, I. *Chem. Phys. Lett*. **1994**, *218*, 343.

(27) North, S. W.; Marr, A. J.; Furlan, A.; Hall, G. E. *J. Phys. Chem. A* **1997**, *101*, 9224.